Influence of Diffuse and Ground-Reflected Irradiance on the Spectral Modeling of Solar Reference Cells

Frank Vignola[1], Josh Peterson[1], Rich Kessler[1], Sean Snider[2], Peter Gotseff[3], Manajit Sengupta[3], Aron Habte[3], Afshin Andreas[3], and Fotis Mavromatakis[4]

[1]Material Science Instituted/University of Oregon, Eugene (USA)
[2]St. Mary's High School, Medford (USA)
[3]National Renewable Energy Laboratory, Golden (USA)
[4]Department of Electrical and Computer Engineering/Hellenic Mediterranean University, Heraklion (Greece)

[a)] Corresponding author: Frank Vignola: fev@uoregon.edu
[b)] Josh Peterson: jpeter4@uoregon.edu

1. Abstract

An enhanced model is introduced to estimate reference cell output on a two-axis tracking surface using measured spectral irradiance and reference cell temperature. The model also uses the reference cell spectral responsivity and the spectral temperature responsivity. Under clear skies in July and December, the model reproduces reference cell measurements with an uncertainty of 0.9% at the 95% level of confidence. Under cloudy conditions during July the modeled results match the measured data with an uncertainty 4.5% at the 95% level of confidence and in December, the difference was 5.3%. These uncertainties are over a range of solar zenith angles from 20° to 85°.

Keywords: Reference cell, spectral radiation, modeling

2. Introduction

As larger photovoltaic (PV) systems are installed it is becoming more important to monitor the system performance and to identify changes in performance to quickly address potential problems as they arise. This can be done using high-quality pyranometers or solar reference cells. Reference cells are similar to miniature solar panels being constructed with the same material as the PV panel and using the same glazing and anti-reflection coating as the panel. The only difference between the reference cell and the PV panel is that the reference cell operates at the short-circuit current and the PV panel in the array operates at the maximum power point. Because the relationship between the short-circuit current and the maximum power point is well understood and characterized, models exist relating reference cell measurements with PV system performance. The relationship between incident radiation, measured by the pyranometer, and the PV system performance is complex because the spectral distribution of the incident radiation and the angle-of-incident (AOI) effects must be considered; therefore, reference cell measurements in the plane-of-array of the PV panels are often used to monitor PV system performance because the reference cells are similarly affected by spectral distribution and AOI effects.

Said another way, reference cells do not make good pyranometers because reference cells exhibit significant spectral and AOI dependencies. These are similar to the dependencies that PV panels exhibit and they must be modeled if pyranometers are used to measure the incident radiation; therefore, comparing reference cell measurements to pyranometer readings requires significant modeling efforts to adjust the reference cell measurements to standard conditions. As used here, *standard condition*s mean a solar zenith angle (SZA) of 45°, a standard irradiance spectral distribution, and a temperature of 25°C. These are conditions that are used to determine the calibration of a pyranometer. A perfect pyranometer does not significantly change its calibration values as the SZA, spectral distribution, and temperature change. All pyranometers do have some dependence on SZA, incident spectral distribution, and temperature, but these systematic biases are only a few percent of the measurement. For reference cells, changes with SZA, temperature, and spectral distribution are significant and, therefore, it is difficult to use reference cell measurements to analyze PV systems at different tilts and orientations. First, a model would be needed to adjust the reference cell measurements to standard conditions, and then a companion model would be needed to adjust the values at standard conditions to the appropriate values at the new tilt, orientation, SZA, spectral distribution, and temperature.

Improved estimates of PV system performance require detailed information on the amount and characteristics of the irradiance on the solar cells. Reference cells provide a controlled basis to characterize the spectral, AOI, and temperature effects on the performance of PV panels and systems. On a two-axis tracking surface during clear periods, a very consistent relationship between spectral irradiance and reference cell performance has been shown using a simplified model (Vignola, et, al. 2017a, 2017b, Vignola, et. al, 2018, Vignola, et. al, 2021, Vignola, et. al., 2020). In the simple model it was assumed that spectral beam normal irradiance (BNI) and diffuse and ground-reflected irradiance behaved the same under clear skies. Under cloudy skies, for a two-axis tracking surface, the use of this simple model exhibited a 2% to 3% percent shift in the measured output.

3. Simple Reference Cell Spectral Model

The relationship between the measured spectral irradiance (I_λ) and the estimated reference cell measurement (RC_{Model}) is given in eq. 1.

$$RC_{Model} = K \cdot \int R_\lambda \cdot I_\lambda \cdot T_\lambda \cdot (T_{rc} - 25℃) \cdot F(AOI) \cdot d\lambda \qquad \text{(eq. 1)}$$

where R_λ and T_λ are the reference cell spectral responsivity and the spectral temperature sensitivity of the reference cell. T_{rc} is the temperature of the reference cell and F(AOI) is the AOI effect of the reference cell. The constant, *K*, is related to the calibration of the reference cell and is necessary because the reference cell spectral responsivity is obtained from the relative quantum efficiency, and *K* is only obtained only through measurement or calibration. If all the values in eq. 1 were precisely known, then *K* would be a constant under all conditions.

A two-axis tracking surface was selected for this study because the incident radiation, during sunny periods, is mostly normal to the surface and AOI effects are minimized. In an earlier study Vignola, et al., (2020), it was assumed that F(AOI) for a two-axis tracking surface from BNI, diffuse, and ground-reflected irradiance was equal to 1 for all wavelengths. For BNI, this is true because normal incident light passes through a glass glazing (Marion, 2017). For diffuse and ground-reflected irradiance this is not true and the transmission depends on the nature of the diffuse and ground-reflected irradiance (Marion, 2017).

This paper builds on previous work (Vignola et al., 2020) but incorporates a realistic F(AOI) for the diffuse and ground-reflected contributions by separating the diffuse irradiance into circumsolar, sky dome, and horizontal brightening components and by using a transmission model (Marion 2017) to estimate the diffuse and ground-reflected AOI effects. In fact F(AOI) has some wavelength dependencies, but for this analysis, it is assumed to be independent of wavelength.

The main goal of this work is to evaluate the improvement to the simple reference cell model when a realistic F(AOI) for diffuse and ground-reflected irradiance is taken into account. How much does the inclusion of diffuse and ground-reflected irradiance affect the model results under clear and cloudy sky conditions? The model for the diffuse and ground-reflected irradiance comes from Marion (2017), and the separation of the diffuse irradiance into the circumsolar, dome, and horizon brightening comes from Perez et al. (1990).

The data for this study comes from two spectroradiometers and a reference cell mounted on a two-axis tracking surface at the National Renewable Energy Laboratory (NREL) in Golden, Colorado at the Solar Radiation Research Laboratory (SRRL). Only two months will be studied—July 2020 and December 2020—to illustrate the universality of the results and to examine whether the reference cell and enhanced model behave in a similar manner throughout the year. Initially, clear-sky results are evaluated. In the following section, the results during cloudy periods are examined. The results of the comparisons are then discussed, followed by the next steps needed to evaluate the usefulness of this simple model for other fixed and tracking surfaces.

4. Spectral and Reference Cell Data at SRRL

The data used in this study comes from an IMT solar reference cell and two EKO spectroradiometers mounted on a two-axis EKO tracker (See Figure 1). Several other reference cells—Li-Cor 200R, a Kipp & Zonen SP Lite2 pyranometer, and a Kipp & Zonen CMP22 reference pyranometer—also collect data from the same platform. The two spectroradiometers at the SRRL measure spectral radiation from 300 nm–1650 nm. Data from these instruments have been used in earlier studies (Vignola et al. 2017b, Vignola et al., 2018, Vignola

et al., 2021, Vignola et al., 2020) and can provide a test of the enhanced model in the current study when it is applied to diffuse surface orientations and reference cells.

The experimental setup at the SRRL is shown in Figure 1. The two EKO spectroradiometers are shown by the blue arrows. The IMT reference cell highlighted in this study is shown by the red arrow. The other three reference cells are shown by the green arrows.

Data collection on the two-axis tracker started in May 2020 at the SRRL. All data are reported in 1-minute intervals and some instantaneous data are also available. The spectral data takes from 0.1 to 5 seconds to gather and are stored at the top of the minute. All other instruments are scanned once every 3 seconds and the average measurement is recorded at the ending time. To match the time period of the spectral data, sampled data from the reference cells are used in this study. The difference between the averaged and sampled data is small under clear skies, but it can be significant under cloudy skies where irradiance can vary significantly during short intervals.

Fig. 1. Experimental equipment at the SRRL in Golden, Colorado

Although the pyranometers are calibrated at standard operating conditions, the spectroradiometers are calibrated under laboratory conditions with the light source directly overhead. The directional response and spectral response of the pyranometers are well documented. The difference between the responsivity of the pyranometer under standard conditions when the SZA is near 45° and when the sun is directly overhead (0°) is small. The directional response of the spectroradiometers is larger than for the reference pyranometers, and it has been documented in laboratory conditions, but high-quality field evaluation of the directional response of the spectral radiometers are limited. The directional response of the reference cells is considerable and is evaluated in previous studies (Vignola, et al., 2017a, 2017b, Vignola, et. al., 2018, Vignola, et. al., 2021, Vignola, et. al., 2020).

5. Model Assumptions

In Vignola, et al., (2020) the F(AOI) for all irradiance components was assumed to be the *F(AOI)* for the BNI component and set equal to 1. As an enhancement to this simple model, the F(AOI) for each radiation component was calculated. *The F(AOI)* for each component was assumed to be independent of the spectral irradiance. This assumption is an approximation and the transmission of light through a glazing is slightly dependent on the wavelength (Marion, 2017). The enhanced model also assumes that the Perez model and the Marion model adequately represent the various irradiance components.

The validity of these assumptions can be tested by comparing the ratio between the measured and the modeled reference cell output at different times of year and under different conditions. A model with little bias would produce a ratio that is independent of time of year and SZA.

6. Evaluations Under Clear Skies

In this section, the reference cell output is modeled under clear-sky conditions using the measured relative spectral response of the reference cell, the spectrally dependent temperature response of the reference cell, the measured temperature of the reference cell, and the spectral irradiance from the spectroradiometers. In the earlier simplified model, all irradiance was assumed to be normal irradiance (Vignola, et al., 2020). The enhanced model separates the incident radiation into its components using the Perez model (Perez, et al., 1990). The incident radiation components are: beam normal irradiance (BNI), ground-reflected irradiance (DTI_{GR}) and diffuse irradiance which are further separated into three components, the circumsolar irradiance (DTI_{CS}), the sky dome irradiance (DTI_{Dome}), and the horizons brightening component ($DTI_{Horizon}$). The modeled DTI (DTI_{calc}) is given in eq. 2.

$$DTI_{calc} = DTI_{CS} + DTI_{Dome} + DTI_{Horizon} + DTI_{GR} \quad \text{(eq. 2)}$$

To simplify the terminology in the paper, the sum of the ground-reflected and diffuse components on the surface is referred to as the diffuse tilted irradiance (DTI) which in this study is the diffuse and ground-reflected irradiance on the two-axis tracking surface.

Although the F(AOI) term can be calculated for each component using (Marion, 2017), the spectral distribution of the irradiance that comprises each component is not measured. Although it is theoretically possible to model the spectral contribution of each component, this is complex, depends on high-quality measurements of the atmospheric components, and carries considerable uncertainties. Therefore, to simplify the calculations for the enhanced model, it is assumed that the components have identical spectral distributions equal to the average spectral distribution. This assumption allows one to use the Perez model (Perez et al., 1990) and the Marion model (Marion, 2017) to estimate the average F(AOI) and include the effects of the diffuse and ground-reflected contributions to the overall average F(AOI*)*.

For a two-axis tracking surface, always facing the sun, DTI can be obtained from the global irradiance on the tilted surface (*GTI*) and BNI.

$$DTI = GTI - BNI \quad \text{(eq. 3)}$$

DTI includes both the diffuse and ground-reflected components. DTI obtained using eq. 3 is referred to as DTI_{Meas}. . For the two-axis tracking surface the term Global Normal Irradiance (GNI) will be used instead of GTI. The $F(AOI)_{avg}$ used in the enhanced model is given by eq. 4:

$$F(AOI)_{avg} = \frac{BNI \cdot F(AOI)_{BNI} + DTI_{Meas} \cdot F(AOI)_{DTIavg}}{BNI + DTI_{Meas}} \quad \text{(eq. 4)}$$

where $F(AOI)_{BNI}$ for the *BNI* equals one. $F(AOI)_{DTIavg}$ is given in eq. 5:

$$F(AOI)_{DTIavg} = \frac{DTI_{CS} \cdot F(AOI)_{CS} + DTI_{Dome} \cdot F(AOI)_{Dome} + DTI_{Horizon} \cdot F(AOI)_{Horizon} + DTI_{GR} \cdot F(AOI)_{GR}}{DTI_{Calc}} \quad \text{(eq. 5)}$$

When determining the $F(AOI)_{DTIavg}$ the sum of the DTI components times the appropriate F(AOI) for each component is divided by DTI_{Xalc} because the DTI components sum to DTI_{Calc} and not DTI_{Meas}. Therefore DTI_{Calc} is the proper denominator.

Figures 2a compares the DTI obtained from the measured GNI – BNI against the DTI calculated using the Perez model for July 1, 2020, a clear day. Figure 2b compares the measured and modeled DTI on December 4, 2020, another clear day.

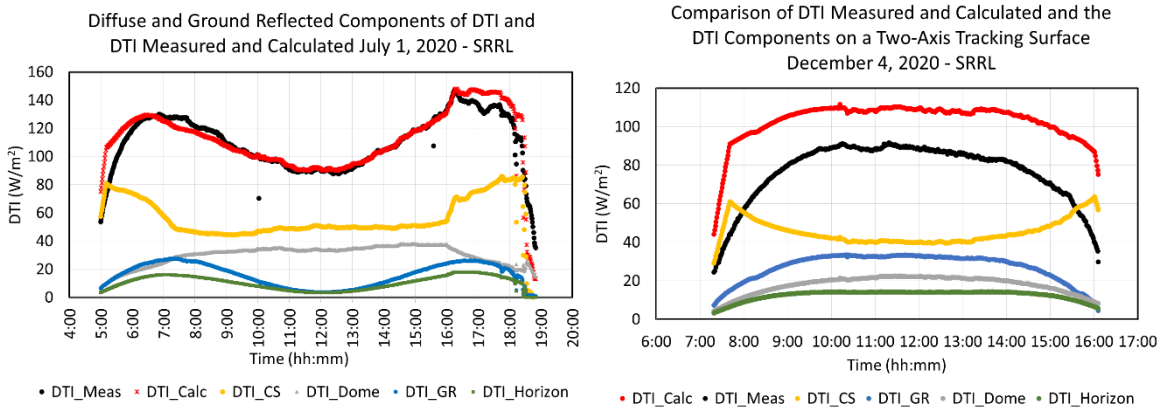

Figs: 2a & 2b: The measured DTI, obtained by subtracting BNI from GNI, are the black points. The DTI_Dome are the gray points, DTI_GR are the blue points, the horizon brightening DTI_Horizon are the green points, and the circumsolar DTI_CS are the yellow points. The calculated DTI is the sum of the components and is shown as the red points.

The measured and modeled DTI in July are a close match. This is not the case for the clear day in December, where the modeled DTI_{Calc} is significantly higher than the measured DTI_{Meas}. This comparison was confirmed by Marion (2021) using NREL's implementation of the Perez model. The DTI components are calculated from measured GHI from a Kipp & Zonen CMP22 pyranometer as well as the measured DHI. Surface albedo was measured using a Kipp & Zonen CM11 pyranometer. No consistent explanation was determined for the difference between the modeled and measured DTI (DTI_{Calc} and DTI_{Meas} respectively); therefore, in order to estimate the average $F_{avg}(AOI)$, the calculated DTI terms were weighted by the DTI_{Calc} and this $F_{avg}(AOI)$ was used with the DTI_{Meas} in the final calculations (see eqs. 4 and 5).

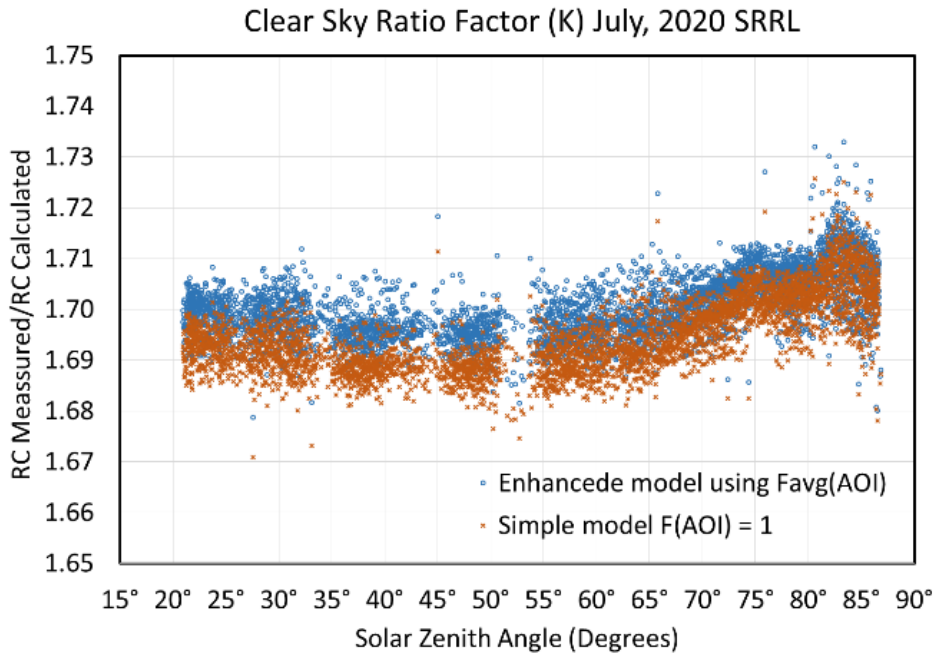

Fig. 3a: Comparison of the ratio factor K the ratio of the reference cell measurements to the calculated reference cell values assuming that the $F(AOI)_{DTIAVG}$ = 1 and with modeled $F(AOI)_{DTIavg}$ during sunny periods in July at the SRRL. Periods when the clouds represented less than 15% of the total sky cover were selected as clear skies.

In the simple model under clear skies, the K factor or ratio—the measured reference cell output divided by calculated reference cell output—was determined using the assumption that F(AOI) was always one and $F(AOI)_{avg}$ was used by the enhanced model in calculating the ratio (K' in the following plots). The $F(AOI)_{avg}$ is always less than one because a portion of any incident radiation not coming at a perpendicular angle to the surface of the glazing will be reflected or absorbed. This was done for July 2020 and December 2020 (See Figures 3a and 3b).

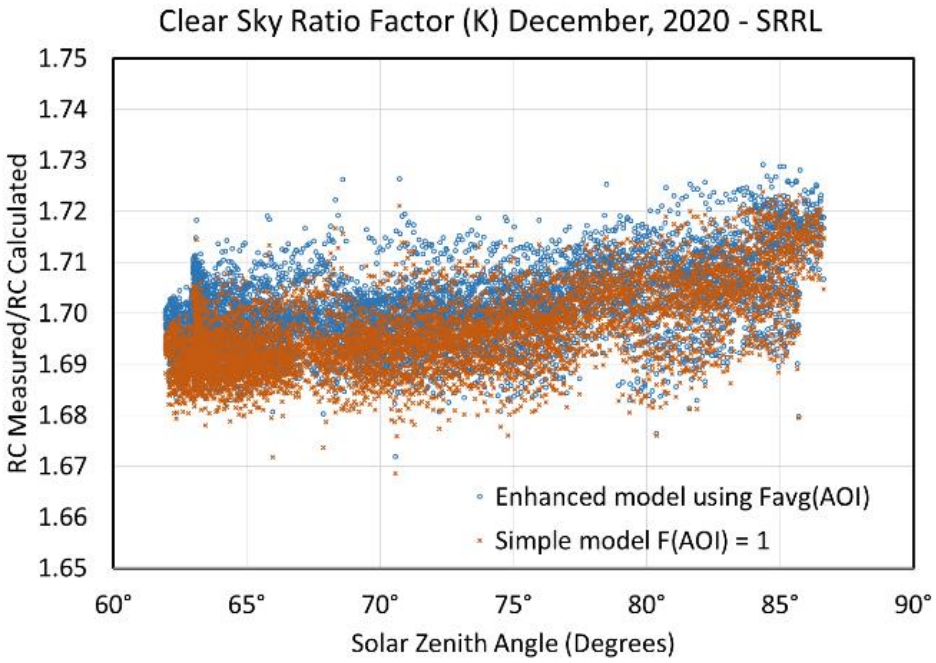

Fig. 3b: Comparison of the ratio factor K the ratio of the reference cell measurements to the calculated reference cell values assuming that the $F(AOI)_{DTIAVG}$ = 1 and with modeled $F(AOI)_{DTIavg}$ during sunny periods in December at the SRRL. Periods when the clouds represented less than 15% of the total sky cover were selected as clear skies.

The summer and winter clear-sky data shown in Figures 3a and 3b were vetted by removing the BNI that showed significant reductions from the nearby BNI values. In addition, data with negative DTI values were eliminated. Typically, this happens when the GNI sensor is shaded but the BNI sensor is not. With the vetted data, the small increase in the K values at large zenith angles becomes apparent. During July, the average K values was 1.695 with a standard deviation of 0.007 and the average K' value that included the $F(AOI)_{DTIavg}$ was 1.701 with a standard deviation of 0.006. The inclusion of the $F(AOI)_{DTIavg}$ contribution increased the ratio by 0.3%. In the winter, the simple model ratio values (K) were 1.696 with a standard deviation of 0.008 and the ratio values adjusted for the enhance model using $F(AOI)_{DTIavg}$ were 1.701 with a standard deviation of 0.008. Inclusion of the $F(AOI)_{DTIavg}$ contribution increased the ratio by 0.3%.

7. Evaluation Under Cloudy Skies

Under cloudy skies, the inclusion of the $F(AOI)_{DTIavg}$ values is expected to have a larger influence on the $F(AOI)_{avg}$ values because the BNI contribution is significantly reduced and the $F(AOI)_{DTIavg}$ values are less than 1. To show the effect of including the $F(AOI)_{DTIavg}$ values under cloudy conditions, the ratio of the reference cell measurement divided by reference cell's calculated output (K) was compared to the same ratio where the calculated reference cell values were adjusted to include the $F(AOI)_{DTIavg}$ contributions (K'). To examine periods when the sky was most covered with clouds, only data collected when the cloudiness factor was 85% or higher were used. These values are shown in Figures 4a and 4b for July and December 2020 at the SRRL in Golden, Colorado.

For the July data, the unadjusted K value averaged 1.653 with a standard deviation of .039. For the K' value that included the calculation of the $F(AOI)_{DTIavg}$ effect on the average F(AOI), the average K' was 1.699 with a standard deviation of 0.037. The effect of the $F(AOI)_{DTIavg}$ factors reduced the average F(AOI) by approximately 2.7%. To help ensure that the cloudy periods were examined, only data obtained when BNI was less than 500 Wm^{-2} were used.

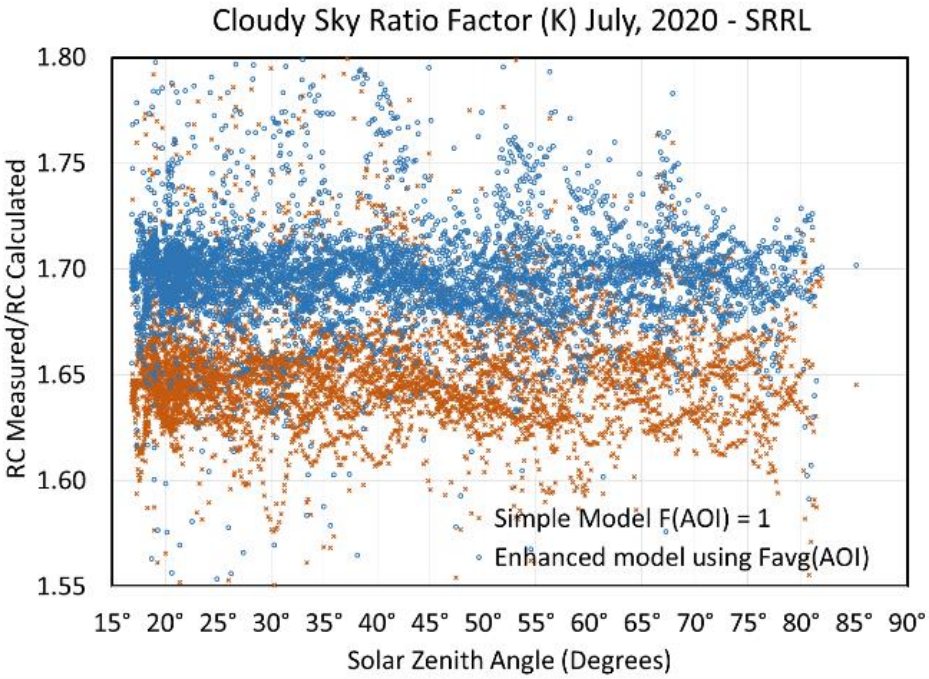

Fig. 4a: Comparison of the ratio of measured reference cell output to the calculated reference cell values during cloudy weather when the percentage cloudiness was 85% or greater for July at the SRRL. The plots contain information on the K value obtained with and without including the $F(AOI)_{DTIavg}$ factor.

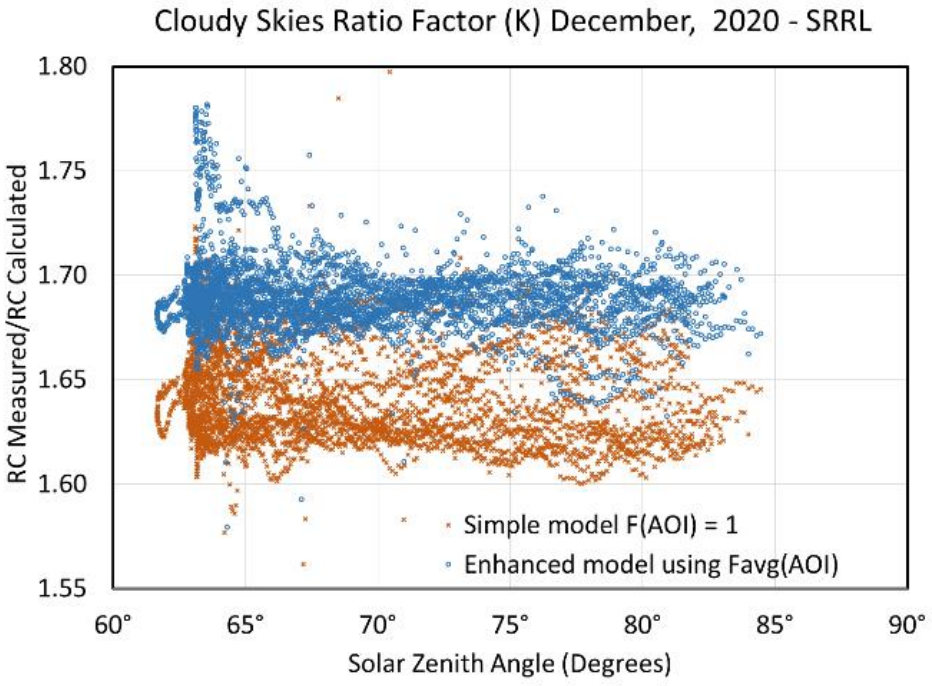

Fig. 4b: Comparison of the ratio of measured reference cell output to the calculated reference cell values during cloudy weather when the percentage cloudiness was 85% or greater for December at the SRRL. The plots contain information on the K value obtained with and without including the $F(AOI)_{DTIavg}$ factor.

During December for cloudiness greater than 85%, the simple model average K ratio was 1.638 with a standard deviation of 0.045 and the enhanced model with the adjusted K' ratio was 1.686 with a standard deviation of 0.042. The inclusion of the $F(AOI)_{DTIavg}$ values increased the ratio by 2.9%. The maximum BNI values under cloudy skies were less than 325 Wm^{-2}. Periods with negative DTI values were not included.

8. Discussion

A simple model for reference cell performance on a **two-axis tracking surface** using spectral irradiance and reference cell temperature measurements is enhanced by including the AOI effects of the diffuse and ground-reflected irradiance values (DTI). Although the F(AOI) value for the BNI irradiance is equal to one (Marion, 2017), the average F(AOI) for DTI irradiance is less than one. Therefore, the average F(AOI) value is slightly less than one under clear skies and is reduced by 2.5% to 3% for totally cloud-covered skies where the DTI term is dominant.

For circumsolar irradiance, the largest contributor to the DTI under clear skies, the F(AOI) was modeled as one. This is an excellent approximation because the transmission of light through the glazing does not change significantly for AOIs less than 30°. For sky dome irradiance, the average transmission of light is approximately 95%. Transmission of light through the glazing from horizon brightening and ground-reflected irradiance depend on the AOI (see Vignola et al., (2020), Marion, (2017) for more detailed information).

The practicality of the enhanced reference cell model depends on how well the calibration constant (K' in this study) of the reference cell remains constant over all circumstances. Of course there will be variation as with any measurements, but if all the systematic biases are appropriately modeled, the ratio between the measured and the calculated reference cell output would be a constant under all circumstances. If assumptions are only partially correct, changes with the average ratio would be observed over different temperature, SZA, or cloud conditions.

Under clear-sky conditions, the inclusion of F(AOI) from the DTI contributions, increased the ratio of the measured to the modeled reference cell output by 0.3% for the IMT reference cell under study. The modeled reference cell output was reduced by the inclusion of the DTI F(AOI) values and hence the ratio of the measured to the modeled was increased. Under clear-sky conditions, the average ratio K' was 1.701 ± 0.012 for July and 1.701 ± 0.016 at the 95% level of confidence. This is very accurate considering this is over a zenith angle ranging from 20° to 85°. There is a slight trend noted with the ratio increased from an average of 1.70 from 20° to 65° to near 1.71 at 85°, or an approximate 0.6% increase over the full SZA range. When the sun is low in the sky, SZA greater than 65°, model assumptions may not be as accurate.

During cloudy or partially cloudy periods there is more variation in the ratios obtained because the instruments see slightly different portions of the sky, and there is difficulty in modeling the DTI components and estimating the *F(AOI)*. The example here used very cloudy skies where the percentage total cloud cover was 85% or higher. Even under heavy cloud cover, the BNI varied from zero to 1000 Wm^{-2}. This represents a wide range of sky conditions. Periods with BNI greater that 500 Wm^{-2} were eliminated to remove periods when the sun shinned through a hole in the clouds. Without including the $F(AOI)_{DTIavg}$, the simple model produced ratios of K that were 2.5% to 3% lower than the results that included the $F(AOI)_{DTIavg}$ in the calculations. Including the $F(AOI)_{DTIavg}$ represents an noticeable improvement in the calculated reference cell measurements; however the uncertainty in the ratio values was approximately 5% at the 95% level of confidence. The difference in the average K' ratio calculated in July during significant cloud cover and under sunny skies was 0.35% at the 95% level of confidence. For the data in December, the difference was 1.6% at the 95% level of confidence. Given the uncertainty of the average K' obtained during cloudy periods from 2.5% to 3%, this is within the uncertainty of the measurements.

One possible source of error in the model estimates likely occurs when the sum of the modeled DTI components were larger than the measured DTI value. To compensate for this difference, the values of all DTI components were adjusted by a constant amount to match the measured DTI value. Because each $F(AOI)_{DTIavg}$ is different, this method treats all DTI components equally and might have resulted in over- or underestimating some of the $F(AOI)_{DTIavg}$ contributions. The largest DTI component is the circumsolar component and it has a $F(AOI)_{CS}$ value equal to 1. Over or underestimating the contribution of DTI_{CS} would certainty affect the $F(AOI)_{avg}$.

9. Conclusions

Given the uncertainty in the spectral measurements and the other measurements used to obtain the DTI components, these results show a very robust model for estimating the measurements of solar reference cells. These results apply to the IMT reference cell on a two-axis tracking surface, and the data are from one location, the SRRL in Golden, Colorado. At least in principle the simple model works well with F(AOI) equal to one under clear skies. Under cloudy skies, the enhanced model that includes the calculated $F(AOI)_{DTIavg}$ provides a more consistent ratio K' value. More work is needed examine the results using different reference cells and on different surfaces where the *F(AOI)* values have a larger variation. For the proposed method to be validated, an improved understanding of reference cells characteristics is needed through enhanced experimental setups.

10. Future Efforts

Four areas of work need to be completed. First, the enhanced method needs to be tested on different reference cells, especially those with a different spectral responsivity. Second, the method needs to be tried at different locations to ensure that the modeling has a universally applicable. Third, the model needs to be tested on different surfaces and orientations. This testing will help examine the *F(AOI)* modeling that was used. Fourth, modeled spectral data needs to be substituted for the measured spectral data to determine the ability of the model to produce useful results at locations where measured spectral data does not exist. Future plans will incorporate these four analyses.

One surprising result of this study was the overestimate of the DTI components during December. This needs to be examined in more detail to determine the cause of this overestimation. Is the cause a result of the data used in the model or the model itself? Neither prospect is the apparent cause of this difference, and more study is needed. Also, use of other models that determine the DTI components needs to be attempted.

Each DTI component has a different spectral signature, and this signature is dependent on the sky cover. For example, under clear-sky conditions, the irradiance of the diffuse dome component peaks in the blue portion of the spectrum. Under cloudy conditions, the peak of the diffuse dome spectral irradiance has a different distribution. How the different spectral distributions of the diffuse components affect the models estimates has not been studied.

When the final results of this project are completed, one should be able to calculate the accuracy of using modeled spectral data to calculate the reference cell output and even the incident radiation. This uncertainty can be translated directly into the uncertainty to which the production of PV power systems can be estimated using modeled spectral data.

11. Acknowledgements

The University of Oregon Solar Radiation Monitoring Laboratory would like to thank the National Renewable Energy Laboratory as well as the Murdoch Family Trust for funding the project. We also thank the other sponsors of the University of Oregon Solar Radiation Monitoring Laboratory, the Bonneville Power Administration, the Energy Trust of Oregon, and Portland General Electric.

This work was authored in part by Alliance for Sustainable Energy, LLC, the manager and operator of the National Renewable Energy Laboratory for the U.S. Department of Energy (DOE) under Contract No. DE-AC36-08GO28308. Funding provided by U.S. Department of Energy Office of Energy Efficiency and Renewable Energy Solar Energy Technologies Office. The views expressed in the article do not necessarily represent the views of the DOE or the U.S. Government. The U.S. Government retains and the publisher, by accepting the article for publication, acknowledges that the U.S. Government retains a nonexclusive, paid-up, irrevocable, worldwide license to publish or reproduce the published form of this work, or allow others to do so, for U.S. Government purposes.

12. References

1. Vignola, F., Chiu, C., Peterson, J., Dooraghi, M.. Sengupta, M., 2017. Comparison and analysis of instruments measuring plane-of array irradiance for one-axis tracking PV systems, IEEE PVSC Conference, Washington D.C., 2017

2. Vignola, F., Peterson, J., Dooraghi, M., Sengupta, M., Mavromatakis, F., 2017.Comparison of Pyranometers and Reference Cells on Fixed and One-Axis Tracking American Solar Energy Society Conference Denver, Colorado October 9–12, 2017
3. Vignola, F., Peterson, J., Kessler, R., Dooraghi, M.. Sengupta, M.,, and Mavromatakis, F., 2018. Evaluation of Photodiode-based Pyranometers and Reference Solar Cells on a Two-Axis Tracking System, World Conference on Photovoltaic Energy Conversion Waikoloa, Hawaii, June 10-15, 2018
4. Vignola, F., Peterson, J., Kessler, R., Sandhu, V., Snider, S., Habte A., Gotseff, P., Andreas, A., Sengupta, M., and Mavromatakis, F., 2021. Improved Field Evaluation of Reference Cell Using Spectral Measurements, Solar Energy 215, 482-491, 2021
5. Vignola, F., Peterson, J., Kessler, R., Snider, S., Andreas, A., Habte A., Gotseff, P., Andreas, A., Sengupta, M., and Mavromatakis, F., 2020. Evaluation of Reference Solar Cells on a Two-Axis Tracking Using Spectral Measurements, SolarPACES, September 27–October 1, 2020
6. Marion, B., 2017. Numerical method for angle-of-incidence correction factors for diffuse radiation incident photovoltaic modules, Solar Energy 147 (2017) 344–348
7. R. Perez, P. Ineichen, R. Seals, J. Michalsky, Modeling daylight availability and irradiance components from direct and global irradiance, Solar Energy 44, 271–289 , 1990
8. B. Marion 2021 (private communication)